Scholars Academic Journal of Biosciences
Abbreviated Key Title: Sch Acad J Biosci
ISSN 2347-9515 (Print) | ISSN 2321-6883 (Online)
Journal homepage: https://saspublishers.com
NLM ID:101629416

OPEN ACCESS

Chemistry

Adsorption of Dye Using Cu Doped Fe_2O_3 Nanoparticles: An Innovative Approach for Effective Wastewater

Sana Shahid[1*], Muhammad Ikrama Shoukat[2], Hafiz Salman Tayyab[3], Naheed Sharif[4], Fatima Muqddas[5], Rohul Amin[6], Malik Salman Tariq[7], Rabiya Bashir[8], Amna Qais[9], Rimsha Aslam[10]

[1]Department of Chemistry, University of Agriculture Faisalabad 38000, Pakistan
[2]Institute of Physics, the Islamia University of Bahawalpur, Pakistan
[3]Department of Applied Science, School of Science, National Textile University Faisalabad
[4]Department of Chemistry, University of Sargodha, Pakistan
[5]Department of Chemistry, University of Okara, Pakistan
[6]Department of Geology, University of Peshawar, Pakistan
[7]Institute of Physics, the Islamia University of Bahawalpur, Pakistan
[8]Department of Botany, University of Agriculture Faisalabad 38000, Pakistan
[9]Department of Chemistry, Punjab University Lahore, Pakistan
[10]Department of Chemistry, University of Agriculture Faisalabad 38000, Pakistan

DOI: https://doi.org/10.36347/sajb.2025.v13i07.014 | **Received:** 01.06.2025 | **Accepted:** 15.07.2025 | **Published:** 31.07.2025

***Corresponding author:** Sana Shahid
Department of Chemistry, University of Agriculture Faisalabad 38000, Pakistan

Abstract | **Original Research Article**

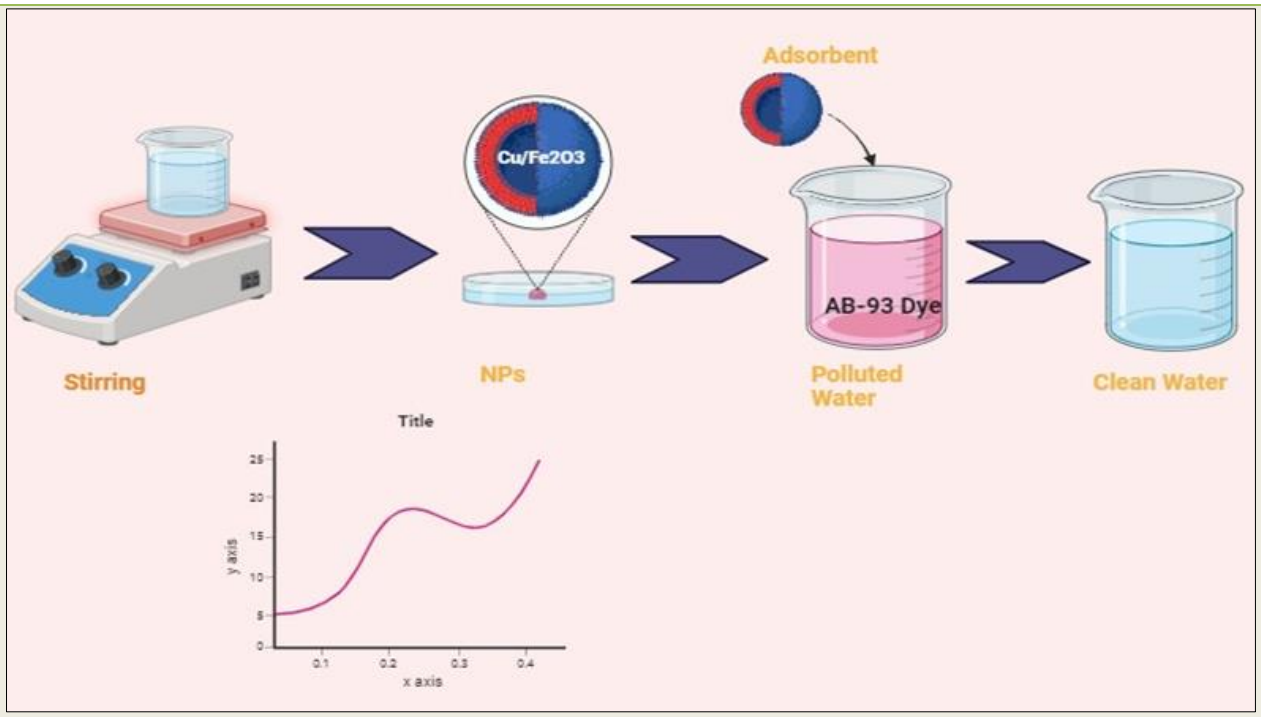

Graphical Abstract

Access to safe drinking water has become more challenging due to daily water pollution worldwide. This study synthesized Cu-doped Fe_2O_3 NPs via the co-precipitation method and demonstrated their excellent adsorption efficiency for dye removal. Cu/Fe_2O_3 NPs effectively removed the synthetic acidic dye Acid Blue 93 under optimized conditions: pH 2, 0.05g/50mL dosage, 90 min, 35°C temperature, and 150ppm Acid Blue-93 dye concentration, achieving higher adsorption capacity of 38.02 mgg^{-1}. Pseudo-second-order and Freundlich adsorption isotherms demonstrated strong fit results concerning the adsorption kinetics and equilibrium data. Thermodynamic parameters confirmed the adsorption process's feasibility. Electrolytes and heavy metal ions influenced adsorption potential, while surfactants reduced

efficiency. 0.5 N NH_4OH and 0.5 N NaOH was found to be the most effective for desorption. FTIR and X-ray diffraction (XRD) have been used to examine the functional groups involved in active binding and crystal structure.

Keywords: Cu Doped Fe_2O_3 Nanoparticles, Adsorption, Acid Blue-93 Dye, Kinetics, Equilibrium, Thermodynamics.

1. INTRODUCTION

Water is a basic human need that is vital to life and strongly related to livelihood and overall health (Sohail *et al.*, 2022). Clean water is essential for human existence and serves as a vital feedstock in many significant industries, including those that produce electronics, drugs, and food (Zhang *et al.*, 2022). The biosphere is affected by challenging obstacles in conjunction with increasing difficulties of pure water as available freshwater resources are reducing as a result of protracted droughts, resident increase, more stringent health-based regulations, and competing needs from a variety of customers. According to studies, just 3% of the water on Earth is genuinely freshwater; the most readily available source of drinking water, water for manufacturing purposes in some areas, and novelty in the development of new ecosystems is seawater (Abel *et al.*, 2021).

One of the most critical environmental problems in the world is water pollution, and industrial wastewater is a significant cause of it. Industrial wastewater's complicated composition, limited biodegradability, and high toxicity can have a significant negative influence on ecosystems (Liu *et al.*, 2021). Wastewater has the ability to measure the load of a range of viruses since viruses can enter waste streams by a number of different channels, including faeces, blood, saliva, skin, and urine. It is widely known that enteric viruses, such as rotaviruses, adenoviruses, enteroviruses, hepatitis A and E viruses, caliciviruses, and others, may be found in wastewater (McCall *et al.*, 2020). The main goal of nanotechnology is to form innovative constructions, procedures, or schemes with enhanced electrical, optical, magnetic, conductive, or mechanical properties by influencing material at the molecular and atomic levels. Water treatment is one area where studying nanotechnology as a potentially beneficial technology has yielded outstanding results (Jain *et al.*, 2021).

Paralleled to pigment-based color repels, dye-based color repels provide a number of benefits. Due to dyes' great solubility in solvents, extra dispersion procedures are typically not needed. Because of their reduced particle masses compared to pigments, they also have excellent transmittance, pure color, and crisp absorption band (Jang *et al.*, 2022). The textile dyeing business produces a lot of colorful waste fluids, making it a significant cause of water pollution. More than 15% of dyes are created in various textile manufacturing processes, which helps to produce colorful wastewater flows (Pirsaheb *et al.*, 2019).

The chemicals found in textile effluent usually include inorganic compounds and colours (Indigonoid dyes, phthalocyanine dyes, xanthene dyes, azo dyes, triphenylmethane dyes, anthraquinonoid dyes, nitrated dyes, and polymethine dyes. These textile dyes threaten ecological systems and public health if not managed appropriately (Deng *et al.*, 2020).

Wastewater holding color is managed utilizing a diversity of adsorbents, including bio-sorbents, carbon-based nano-adsorbents, and polymer-based adsorbents. Due to their outstanding chemical power, small concentration, constructional elasticity, and validity for field level applications, metal doped nanoparticles adsorbents are the topic of a lot of work in the field of adsorption (Muthukumaran *et al.*, 2022). Several techniques have been defined for the synthesis of metal-doped nanoparticles, involving the quick solvothermal way, chemical spray pyrolysis, chemical vapor deposition, sol-gel procedure, hydrothermal methods, easy combustion, and co-precipitation techniques. Particularly, co-precipitation is an easy, cheap method for fabricating easy metal doped nanoparticles (Harish *et al.*, 2022).

Inorganic salts are often crystallized to create inorganic nanoparticles using a range of conventional and cutting-edge techniques, but the straightforward precipitation process still offers some benefits over others, including low cost, high repeatability, and moderate reaction conditions (Sooch *et al.*, 2021). Doping is a method that aids in enhancing the raw materials' potential. It guaranteed that the semiconductor oxides' inherent characteristics are changed by the direct interaction of doping ions with them. There are several uses for metal-doped nanoparticles in industries including biomedicine, catalysis, and electronics. Iron oxide nanoparticles with a Cu dopant are an amazing material for removing natural colorants from wastewater (Haider *et al.*, 2022).

The adsorption procedure has developed many deliberations due to its low cost, ease of use, and environmental affability (Mozaffari Majd *et al.*, 2022). The procedure of adsorption utilizing adsorbents does not manufacture any dangerous composites (Mok *et al.*, 2020). A number of natural and synthetic adsorbents have been investigated for the removal of dyes and other impurities from aqueous systems. The practical application of these adsorbents is limited by their typical disadvantages, which include weak mechanical strengths, difficulties in separability, non-resistance against acid solutions, and limited adaptation to a wide

variety of dye wastes. Nevertheless, they demonstrate good removal effectiveness (Raza *et al.*, 2022).

Doped Iron oxide nanoparticles are of interest to researchers worldwide due to their extremely tiny size, huge specific surface areas, and conveniently accessible active sites. (Aashima *et al.*, 2019) investigated Ce-doped Fe_3O_4 nanoparticles as a possible adsorbent to extract the azo dye from aqueous solutions. (Kiani *et al.*, 2019) reported purpurin dye in solution is removed using Mn-doped Fe_2O_4 nanoparticles as an adsorbent. (Liang *et al.*, 2010) developed Vd-doped Fe_3O_4 exhibits good adsorption in wastewater organic pollutants' decolorization. (Chen *et al.*, 2019) investigated Fe_2O_3 NPs doped with Ni/Co for effective heavy metal removal from wastewater. (Asfaram *et al.*, 2017) using Mn-doped Fe_3O_4 nanoparticles as a new adsorbent, bright colours are simultaneously adsorbed with ultrasonic assistance.

Table 1: Different metal doped Iron Oxide NPs and their efficiency to remove pollutant

Adsorbent	Method	Pollutants	Adsorption Capacity (mg g^{-1})	Isotherm	Reference
Ce-doped Fe_3O_4 NPs	Hydrothermal	Reactive Black 5	84.58	Langmuir	(Aashima *et al.*, 2019)
Mn-doped Fe_2O_4 NPs	Ultrasonication	Purpurin	60	Langmuir	(Kiani *et al.*, 2019)
Vd-doped Fe_3O_4	Precipitation-oxidation	Methylene blue	18.66	Langmuir	(Liang *et al.*, 2010)
Ni/Co-doped Fe_2O_3 NPs	Hydrothermal	Pb	136	Freundlich	(Chen *et al.*, 2019)
Mn-doped Fe_2O_3 NPs	Green Synthesis	Pb	29.56	Langmuir	(Rehman *et al.*, 2022)
Mn-doped Fe_2O_3 NPs	Ultrasonication	Malachite Green	101.215	Langmuir	(Asfaram *et al.*, 2017)

The study takes a fresh perspective and makes a substantial contribution to the fields of nanotechnology and materials science. For this reason, a co-precipitation approach was used to generate Cu-doped Fe_2O_3 NPs for this investigation. Using FTIR and XRD methods, Cu-doped Fe_2O_3 NPs were characterized. This study's main objective is to examine how well Cu-doped Fe_2O_3 NPs adsorb AB-93 dye. The AB-93 parameters for Cu-doped Fe_2O_3 NPs' adsorption kinetics, isotherms, and thermodynamics were established. Additionally, variables like temperature, starting dye concentration, contact time, dosing rate, and pH that impact AB-93's adsorption ability on this adsorbent were investigated. Furthermore, the effects of heavy metals, electrolytes, and surfactants on the synthesized adsorbent's adsorption efficacies were investigated.

2. RESEARCH METHODOLOGY

2.1 Materials

The highest analytical quality chemicals and reagents used in this investigation were acquired from Merck (Germany) and Sigma-Aldrich Chemical Co. (USA). The following are some of the compounds utilised in this study: $FeCl_3 \cdot 4H_2O$, $CuCl_2 \cdot 2H_2O$, NaOH and deoxygenated distilled water were utilized in the fabrication of Cu doped Fe_2O_3 nanoparticles. The Acid Blue-93 dye was purchased from the Faisalabad, Pakistan, local market.

Characteristics of AB 93 dye (Anionic Acid Blue 93) include Molecular formula:

$C_{37}H_{27}N_3Na_2O_9S_3$, Molecular weight: 799.8, Appearance: Dark blue uniform powder, Solubility: Very soluble in water, Color Index Number: 42780, C.A.S Number: 28983-56-4, Nature: Acidic, λmax: 587 nm.

2.2 Synthesis

It was easy to integrate Cu doped Fe_2O_3 NPs using co-precipitation. 9.9 g of $FeCl_3 \cdot 4H_2O$ and 4.2 g of $CuCl_2 \cdot 2H_2O$ were dissolved in 100 ml of distilled water. The salt solution was mixed with 0.2M NaOH to conduct the pH at 11. To accelerate the formation of precipitates, the solution was kept at 80°C for 3 hours. The next day, the precipitates should be rinsed with water and alcohol after allowing the solution sit all-night. The manufactured product was dried for 3 hours at 1200°C and then calcined for almost 3 hours at 350°C to produce Cu doped Fe_2O_3 nanoparticles (Haider *et al.*, 2022).

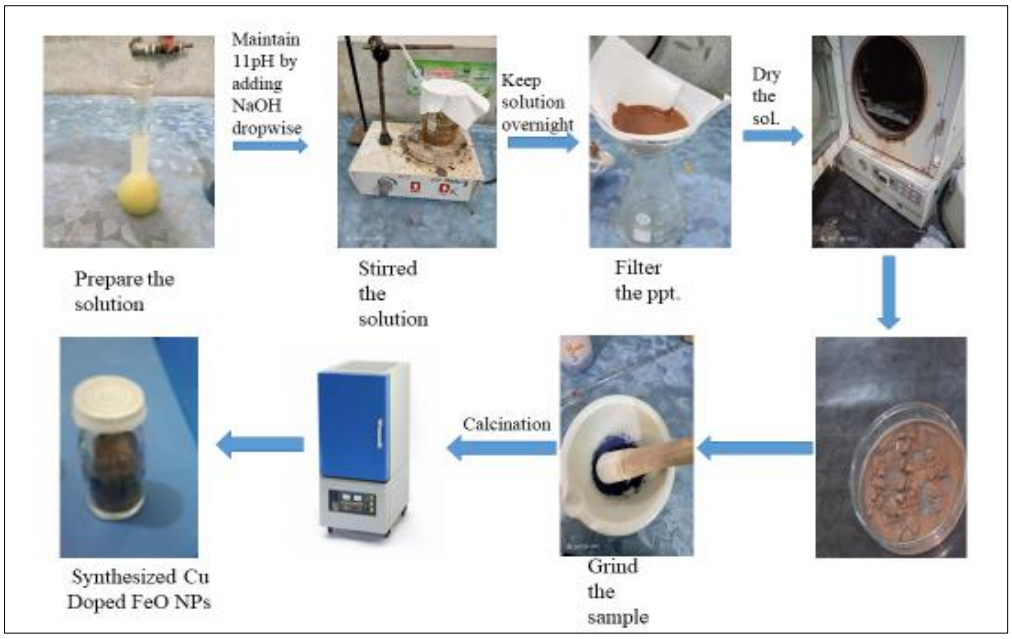

Fig. 1: Schematic diagram of the synthesized Cu Doped Fe_2O_3 NPs

2.3 Preparation of Dye Solution

Anionic dye (Acid Blue 93), which is employed after further purification, was purchased from the Pakistani local market in Faisalabad. In order to create the stock solution, 1g of anionic dye was dissolved in 1000 ml of distilled water in a measuring flask. To create the standard curve, several ppm solutions—10, 20, 30, 40, and 50 ppm—were made from the stock solution using absorption values obtained from a UV spectrometer. After scanning the solutions in the 190–900 nm wavelength range, the λ_{max} for AB 93 dye was determined to be 587 nm.

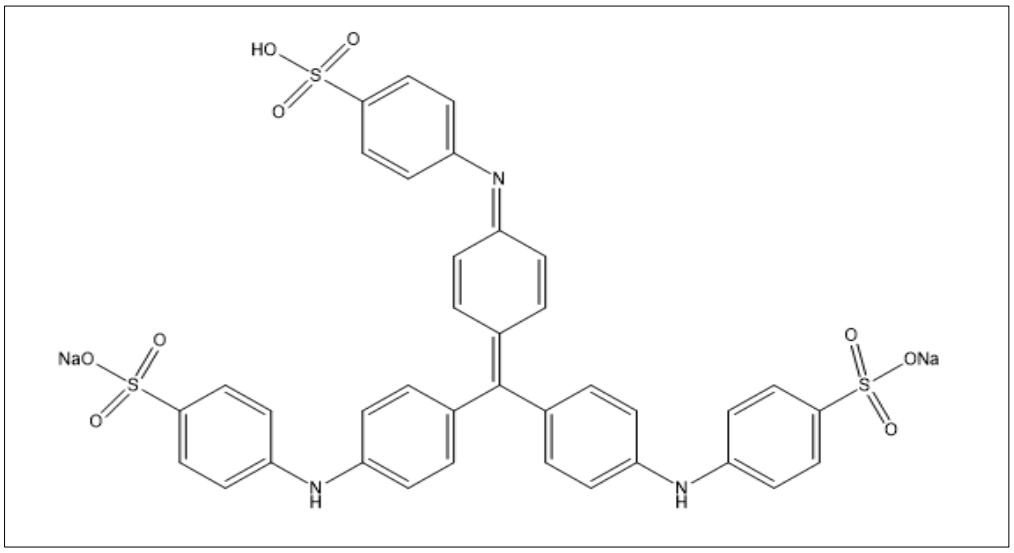

Fig. 2: Structure of selected Acid Blue-93

2.4 Batch Adsorption Experiment

Cu-doped Fe_2O_3 NPs' adsorption properties were evaluated in batch studies using a 250 mL measuring flask that was shaken at 110 rpm. Numerous factors were used to analyse the adsorption of Cu-doped Fe_2O_3 NPs, including pH (2–11), starting dye concentration (10–150 ppm), adsorbent dose (0.05–0.5 g), contact duration (5–90 min), and temperature (30–60 °C). HCl and NaOH were used to regulate the pH of the medium. Every experiment was conducted twice, and the findings were expressed using meanSD. The following relationship was used to compute the equilibrium adsorption uptake, q_e (mg/g):

$$q_e = \frac{(Co - Ce)V}{W} \quad (1)$$

The mass of the adsorbent (g), the volume of the solution (L), the equilibrium dye concentration (mg/L), and the starting dye concentration (mg/L) are represented by C_e and C_o, respectively.

2.5 Effect of Electrolytes

At different salt concentrations, including NaCl, $CaSO_4$, and $CuSO_4$ in 150 mg/L AB 93 dye, the effects of electrolytes were examined. The comparison of all products is then used to calculate the quantity of dye adsorbed on doped nanoparticles.

2.6 The Impact of Surfactants and Heavy Metals

In this work, we investigate how different heavy metal concentrations, such as Cd and Pb, affect Cu/Fe_2O_3 nanoparticles. The impact of surfactants on dye adsorption was assessed using Triton X-100, cetyltrimethylammonium bromide, and SDS in a 1 percent solution, along with the two detergents Excel and Ariel.

2.7 % Desorption

The percentage of desorption is calculated using NaOH and NH_4OH. It states if the adsorbent can be recycled or not.

Percentage dye removal (%)= $\frac{(Co-Ce)}{Co}$ x100 (2)

3. RESULTS AND DISCUSSION

3.1 Characterization of Cu-Doped Fe_2O_3 NPs

3.1.1 FTIR Analysis

The interaction of infrared radiation with particles both before and after the adsorption of the matching acidic dye (AB-93) has been studied using Fourier Transform Infrared Spectroscopy (FTIR). A prominent band can be seen in the Cu doped iron oxide's spectra between 400 and 4000 cm^{-1}. Changes in functional groups impact a compound's chemical and physical characteristics. Because several vibrational frequencies exist that are specific to the presence of certain chemical groups, FTIR may be used to identify them. An extensive peak located between 3225 cm^{-1} and 3229 cm^{-1} illustrates the H_2O stretching on the iron oxide surface. The C=O stretching vibration is established by the peak at 1715 cm^{-1}. Fe–O vibrations were revealed by prominent bands in the FT-IR spectra at 476 cm^{-1} and 544 cm^{-1}. The Cu–O vibrational bands were represented by the band at 602 cm^{-1}.

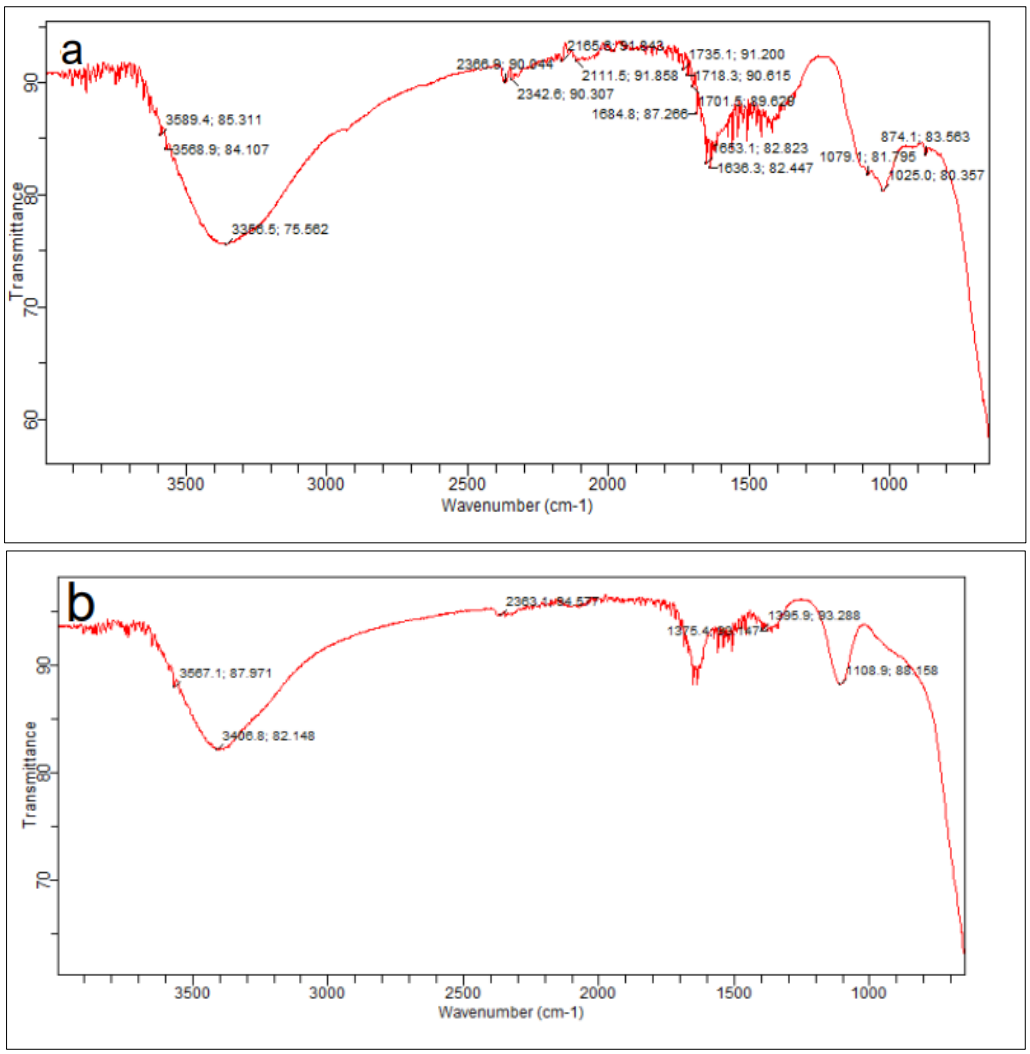

Fig. 3: FTIR spectrum of (a) AB-93 loaded Cu/Fe_2O_3 NPs (b) unloaded Cu/Fe_2O_3 NPs

3.1.2 XRD Analysis

The Cu-doped Fe_2O_3 nanoparticles' XRD pattern was obtained in two theta ranges, 10–70◦. This pattern, which was seen at room temperature, is displayed in Fig. 3. Using the well-known Scherrer formula, Cu-doped Fe_2O_3 NPs were synthesized, and their crystallite size was measured.

$$D = K\lambda / \beta\cos\theta \quad (3)$$

The equation includes the following: D represents the size of the crystallite, K equals 0.9, which is also known as the Scherer constant, λ signifies the X-ray wavelength for a copper source at 1.5406 Å, θ denotes Bragg's angle, and β stands for the Full Width at Half Maximum (FWHM). At 2θ values 35.96◦, 39.24◦, 49.24◦, 60.04◦, and 66.40◦, the peaks are located at planes [110], [006], [024], [214], and [125]. The strong peaks that were gathered show the crystalline shape and high purity of particles. The peak intensities in the Cu doped Fe_2O_3 NPs progressively declined, according to the XRD patterns. The loss of crystallinity and lattice deformation brought on by the higher dopant concentration might be the cause of this fall in intensity. Subsequent examination of the XRD patterns revealed that the peaks were moved to a lower diffraction angle when Cu was added to the Fe_2O_3. This supplied more evidence that Cu^{2+} was present in the host network.

Table 2: Represents the crystallite size of Cu Doped Fe_2O_3 nanoparticles

Peak no.	Peak Position [2θ]	FWHM [◦]	d-spacing [Å]	hkl	Crystallite size [nm]
1	35.96	0.91	2.159	110	91.21
2	39.24	0.96	2.292	006	87.36
3	49.24	0.89	1.840	024	97.21
4	60.04	0.64	1.485	214	142.67
5	66.40	0.74	1.413	125	127.58

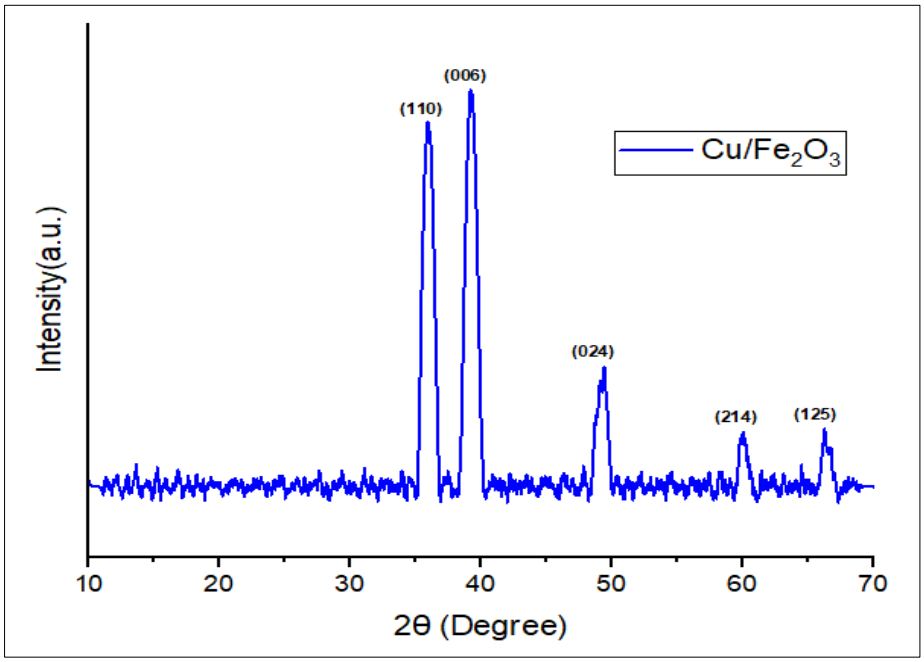

Fig. 4: XRD Analysis of Cu-Doped Fe_2O_3 Nanoparticles

3.2 Calibration Curve

The calibration curves of Acid Blue-93 dye were plotted using solutions of several concentrations created with distilled water. The linear response of the Acid Blue-93 dye calibration curves is fixed using Beer-Lambert's law. According to this law, the absorbance of a substance is directly proportional to its concentration and path length, which leads to a straight-line calibration curve. In the context of Beer-Lambert's law, A represents absorbance, ε is the molar absorptivity coefficient, c denotes the concentration of the analyte, and l indicates the path length; the Beer-Lambert's law equation is represented below.

$$A \in cl \quad (4)$$

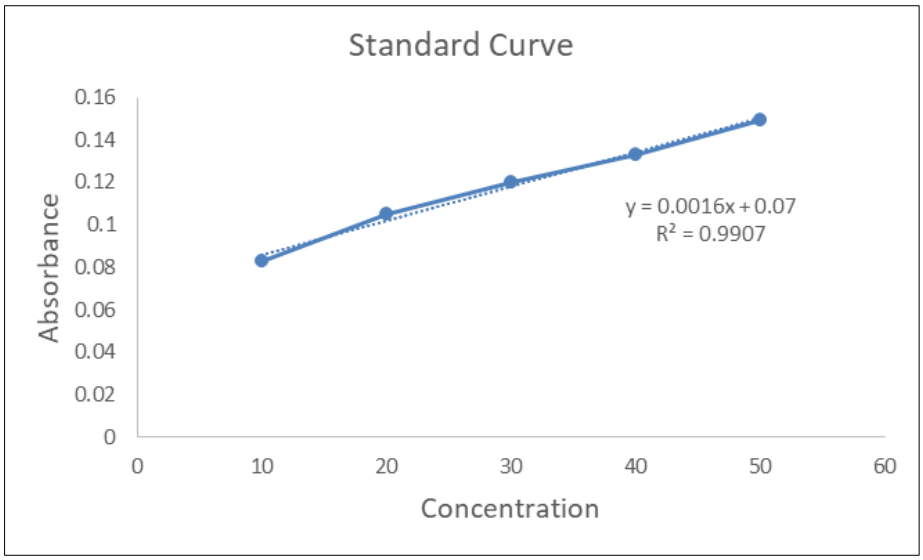

Fig. 5: Calibration curve of Acid Blue-93 dye

3.3 Identifying the Point of Zero Charge (pHpzc)

The pHpzc is an important part employed to check out the ability of the adsorbent on the adsorbent surface and the varieties of active binding sites present. pHpzc works as a helpful standard to create either the surface of adsorbent obtains a +ve or -ve charge respecting to pH levels. Determining the pHpzc of the adsorbent surface is necessary to understand the adsorption mechanism. If pH > pHpzc, cations are more quickly adsorbed, and if pH < pHpzc, anions are more rapidly adsorbed. The solid addition method was used to evaluate the pHpzc of the Cu doped Fe_2O_3 NPs with the highest potential to adsorb Acid Blue 93 dye (El-Habacha *et al.*, 2023).

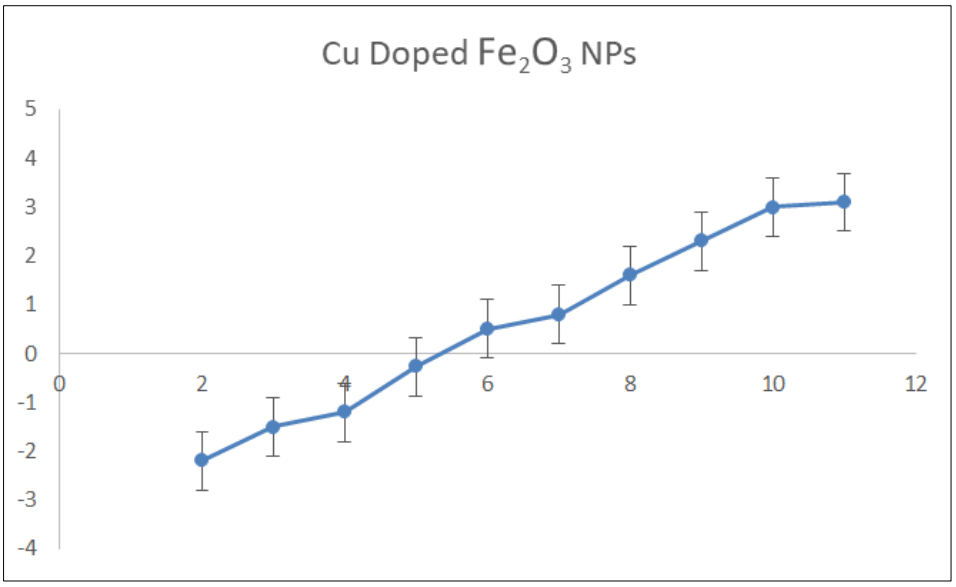

Fig. 6: Point of zero charge

For improved adsorption throughout the testing process, the point of zero charge was altered by introducing 0.1 M NaOH or 0.1 M HCl solution. After transferring 100 mL of aqueous solution to multiple Erlenmeyer flasks, a few drops of 0.1 M HCl or 0.1 M NaOH solutions were added to modify the pH until the required levels were reached. Then, 3 g of Cu/Fe_2O_3 nanoparticles were added to each flask. The final pH was then calculated after 48 hours of agitation at room temperature. The pH at the beginning (pHi) and the pH at the conclusion (pHf) were plotted. By boosting the electrostatic attraction between the adsorbents and dye anions, the elimination of the AB-93 dye is favored by an acidic pH lower than pHpzc. According to the results, Cu/Fe_2O_3 nanoparticles were found to have pHpzc values of 5.7. By protonating surface functional groups below this pH level, the adsorbent gained positive charges and showed electrostatic interaction with dye anions; beyond this pH level, however, the adsorbent created negative charges. Because more positive charges are created on the adsorbent surface when the pH is acidic, there is an increase in the electrostatic interaction

between the AB 93 dye anions and the surface of the adsorbent.

3.4 The pH's Impact

When analyzing the efficacy of adsorbent for color removal, effluent pH is a critical factor. The adsorbent in the solution varies in both ionic form and surface property, altering the dye solution's pH. The function groups on the adsorbent's surface and the dyes' solubility in water may be affected by the pH of the solution. The pH of the adsorbent's immediate environment also affects its rate and activity (Lafi *et al.*, 2019). As part of a continuing scientific study, the anionic Acid Blue 93 dye's pH was tracked from 2 to 11. The color did not alter significantly over the pH range. Operational experimental circumstances, which included a 0.05 g dosage, 50 mg/L, a temperature of 35°C, a shaking speed of 110 rpm, and a contact period of 90 minutes, were used to synthesize Cu/Fe_2O_3 NPs and examine the impact of pH on its activity.

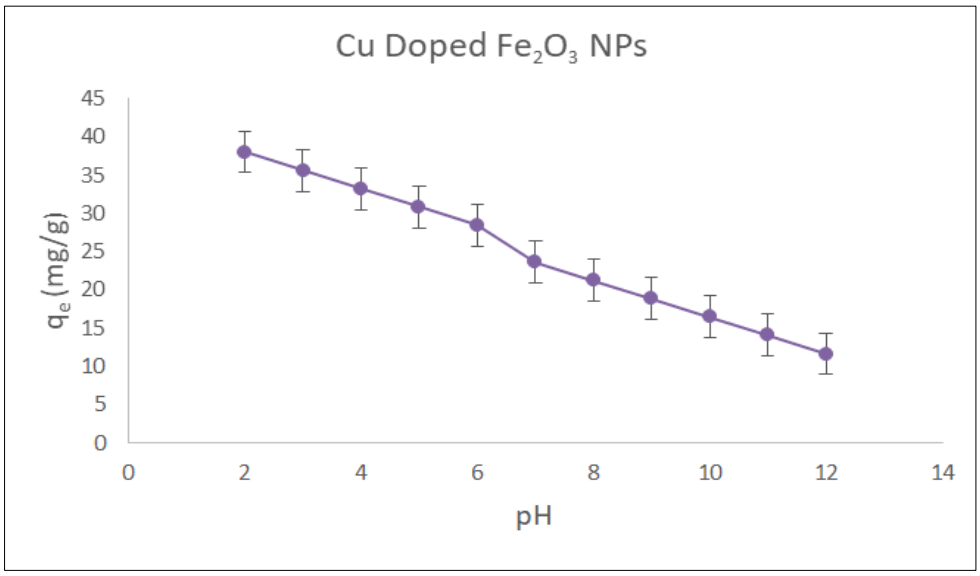

Fig.7: Effect of pH

Figure 7 above illustrates the effect of pH changes on the adsorption capacity of Cu/Fe_2O_3 NPs. With Acid Blue 93 dye removed from the wastewater during treatment, we would have found 0.05 g of dosage, 110 rpm of shaking, 35 °C of temperature, 50 mg/L of initial dye concentration and 90 min of contact time. The qe value for Cu/Fe_2O_3 nanoparticles was 38.02 mgg^{-1}, and the optimal pH was 2. The results above clearly show that the pH of the environment in which the adsorbent is used has a major impact on its ability to remove Acid Blue 93 dye. At pH 2, the maximum adsorption of Acid Blue 93 dye with Cu/Fe_2O_3 nanoparticles. The basic medium was found to have a decreased adsorbent removal capability. An increase in the number of negative charge citations on the adsorbents' surface might be the reason for the removal capacity decrease. A negative interaction between the adsorbents' and the anionic dye molecule's negative charges reduces the adsorption of dye molecules. The solution's pH was lowered to accelerate the anionic dye's adsorption. The rate of adsorption was accelerated by the production of H+ ions at the surface locations of the adsorbents. The electrostatic interaction between positively charged adsorbents and anionic dyes was enhanced by the addition of these ions. This enhanced the capability of the removal.

3.5 Effect of Dose Rate

The dosage, or amount, that is used determines how well an adsorbent works to adsorb substances under specific circumstances. Under continuous operating conditions with an ideal pH of 2, 35°C, 50 mg/L dye concentration, and 110 rpm, Acid Blue 93 dye adsorption was investigated using adsorbent doses (0.05 to 0.5 g/50 mL). The study examined adsorbent concentrations between 0.05 and 0.5 g/50 mL. Fig. 8 displays the findings.

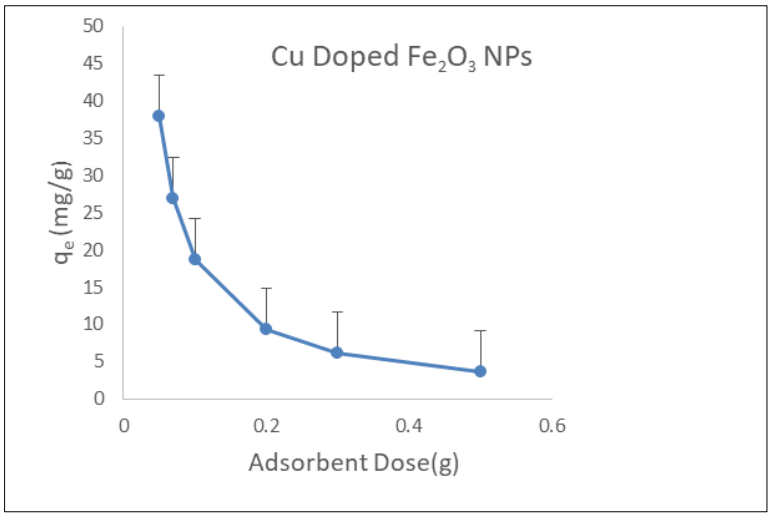

Fig. 8: Effect of Dosage

The adsorption capacity of Cu-doped Fe_2O_3 nanoparticles varies as the adsorbent dosage is raised from 0.05 to 0.5 g while maintaining all other parameters the same. The results demonstrate that a dosage of 0.05 g of Cu/Fe_2O_3 NPs produced the greatest amount of dye elimination. The findings demonstrated that while the availability of unsaturated adsorption sites increased across the diffusional route length, increasing the adsorbent dosage reduced the adsorption of Acid Blue 93 dye. The amount of dye in the finished solution decreased when the adsorbent dose was raised. Because of the strong binding sites that enabled dye molecules to attach, the amount of dye eliminated first rose before leveling out. To prevent the color from diluting in this instance, more adsorbent was applied indirectly. Instead, the availability of functional groups and the amount of accessible surface area were important variables in dye removal. This was determined using an anionic dye that may stick to the surface due to active site overlap. At large doses, this impact resulted in a reduction in the adsorbent's capacity. At higher adsorbent concentrations, the dye molecules' ability to adsorb is diminished because there is not enough adsorbent to cover all of the possible active sites for binding. Since it lowers the amount of solute swallowed, this is another factor causing the adsorption capacity to decrease.

3.6 Impact of Contact Duration

The ability of Cu-doped Fe_2O_3 NPs to absorb and remove dyes is largely dependent on how long they interact with the dye. Adsorption is a characteristic that varies over time and can provide insight into the design and operation of an adsorption system. To clarify the effect of contact time on the adsorption processes, batch adsorption experiments employing Cu-doped Fe_2O_3 NPs with contact durations ranging from 5 to 90 minutes were carried out. This was done in order to determine the best way to effectively remove Acid Blue 93 dye.

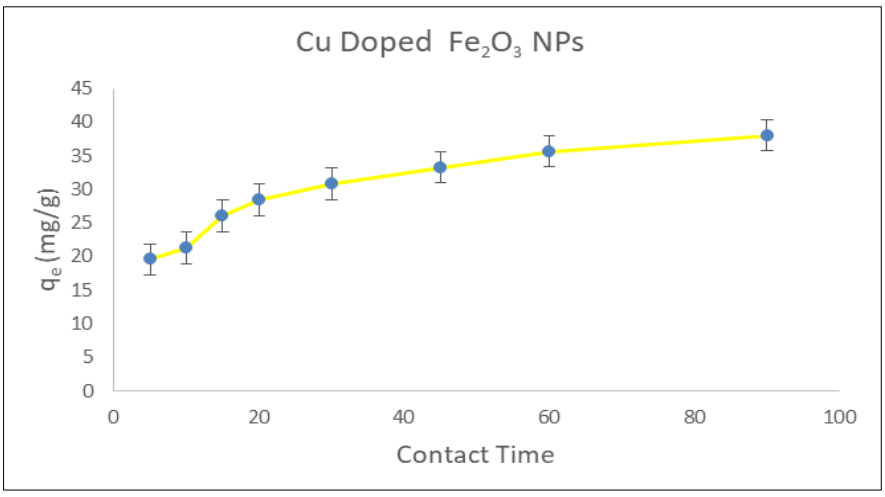

Fig. 9: Effect of Contact time

The adsorption of anionic dye by Cu/Fe_2O_3 nanoparticles began swiftly, slowed down, and after ninety minutes, finally stabilized, based on the results above. Since it was discovered that the adsorption of dye's capacity reached its peak after 90 minutes, the experiment was carried out at that time. The maximal

adsorption capacity remained constant when equilibrium was achieved. The experiment's adsorption rate begins to stabilize and decline after fifteen minutes. The adsorption rate rose as the process moved through its initial phases. The greater surface area, which offers more options for dye molecule attachment, was determined to be the reason of the greatest adsorption rate. As the duration of contact increased, the adsorption rate decreased. Because there were fewer active binding sites available at saturation due to a decrease in surface area, adsorption capacity decreased. Everything returned to normal at this moment.

3.7 Effect of Initial Dye Concentration

The ability of Cu-doped iron oxide nanoparticles to adsorb is greatly affected by the initial concentration of the dye solution. Different concentrations of 10ppm, 25ppm, 50ppm, 75ppm, 100ppm, and 150ppm solutions were generated at optimum pH of 2 for cu doped iron oxide nanoparticles with a 0.05g dose quantity. Although the dye concentration rises, the highest adsorption capability of cu doped iron oxide nanoparticles were recorded at 150 ppm.

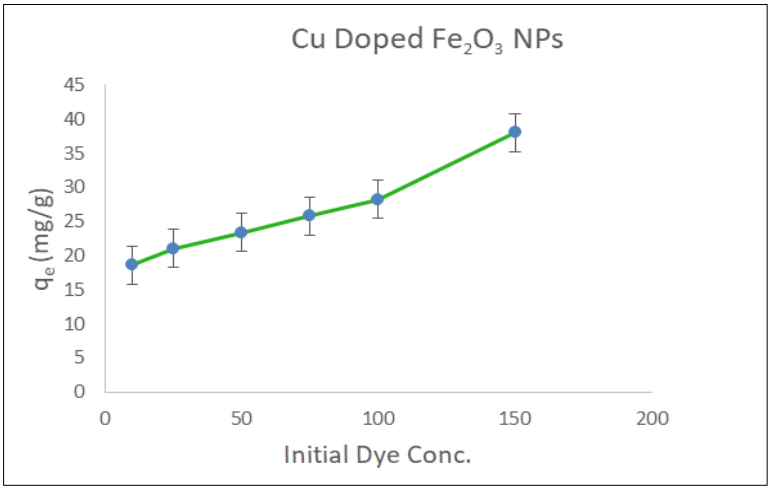

Fig. 10: Effect of Concentration

The % clearance showed a decrease in line with the greater starting dye concentration. This is because the quantity of dye molecules increased as the initial concentration rose and the adsorbent particle was confined. Additionally, the initial rise in concentration impeded the migration of the dye molecule from the bulk solution to the adsorbent surface.

3.8 Temperature Effect

It is crucial to keep in mind that, because textile firms often release their waste at appropriately higher temperatures, temperature may have a significant impact on the dye adsorption processes. Another crucial component for adsorption systems to be effective against real wastes is temperature. The influence of the 30-60°C temperature range on their capacity for adsorption was investigated under closely monitored experimental conditions after an adsorbent was selected to remove anionic dye from industrial wastewater.

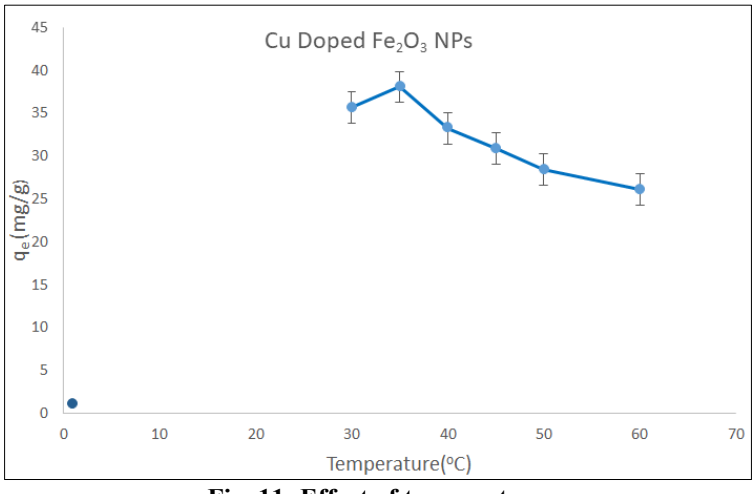

Fig. 11: Effect of temperature

The graph above illustrates how temperature changes impact an adsorbent's capacity to take up biological molecules. At 35°C, Cu/Fe_2O_3 nanoparticles have their maximum adsorption capability. A physiochemical mechanism led to an exothermic temperature rise. As the temperature rose, the process generated less heat due to this reduction in adsorption capacity. Because the adsorptive interactions between the active sites and the dye molecules or species diminish with increasing temperature, less adsorption occurs on the surface of the adsorbent.

Table 3: Represents the optimal conditions for the removal of AB-93 dye

Solution's pH	2
Adsorbent dose	0.05g
Reaction Time	90 min
Initial Dye Conc.	150ppm
Temperature	35°C
Point of Zero Charge	5.7
Shaking Speed	110 rpm

3.9 Kinetic Studies

A significant characteristic that offers valuable insights into reaction pathways and potential uses is the absorption of adsorbates. Various kinetic models, including first-order, second-order, and intra-particle diffusion, have been applied to examine the adsorption process by using absorbance data of the Acid Blue-93 dye with different adsorbents.

3.9.1 Pseudo-First-Order

The first-order can enable simplification of the absorption phenomena. Below is a linear integrated equation of pseudo 1st order: (Lagergren, 1898).

$$\log (q_e - q_t) = \log q_e - K_1 t/2.303 \quad (5)$$

In this context, the symbol k_1 represented the pseudo1st order rate constant. The variable T represents time (in minutes). The theoretical values for q_e and k_1 were obtained by graphing $\log(q_e - q_t)$ against time (t), and they were then computed from the slope and intercept (Yildiz *et al.*, 2023).

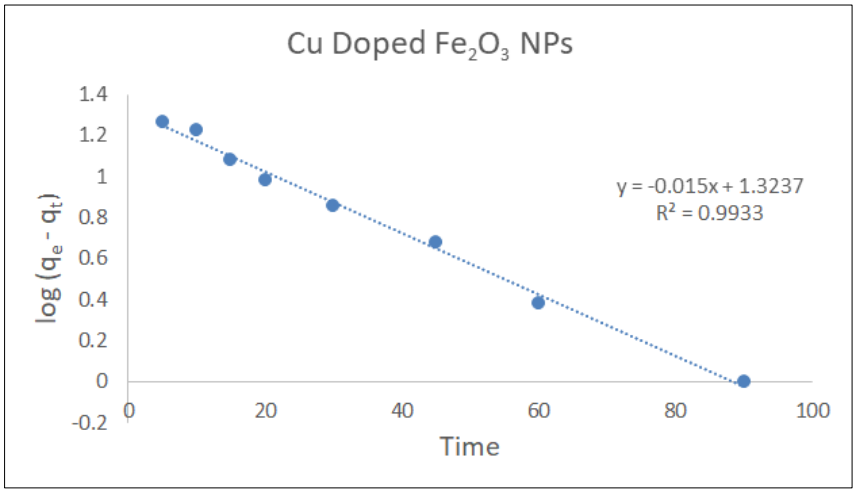

Fig. 12: pseudo-1st Order Model

3.9.2 Pseudo-Second-Order

Utilizing second-order analysis effectively enables a thorough understanding of the absorption procedure over the whole contact time. The following is the 2nd order differential equation:

$$dq_t/dt = K_2 (q_e - q_t)^2 \quad (6)$$

In this context, k_2 stands for the 2nd order rate constant for the asorption process. After analyzing the interaction and applying the boundary conditions, the 2nd order linear form is provided as

$$t/qt = 1/K_2 qe_2 + t/qe \quad (7)$$

The 2nd order rate constant, k_2, along with the intercept and slope, can be determined by creating a plot of t/q_t against t (Tran, 2023). The values for R^2, K_2, and qe cal regarding the adsorption of Acid Blue-93 using cu-doped iron oxide nanoparticles are provided below.

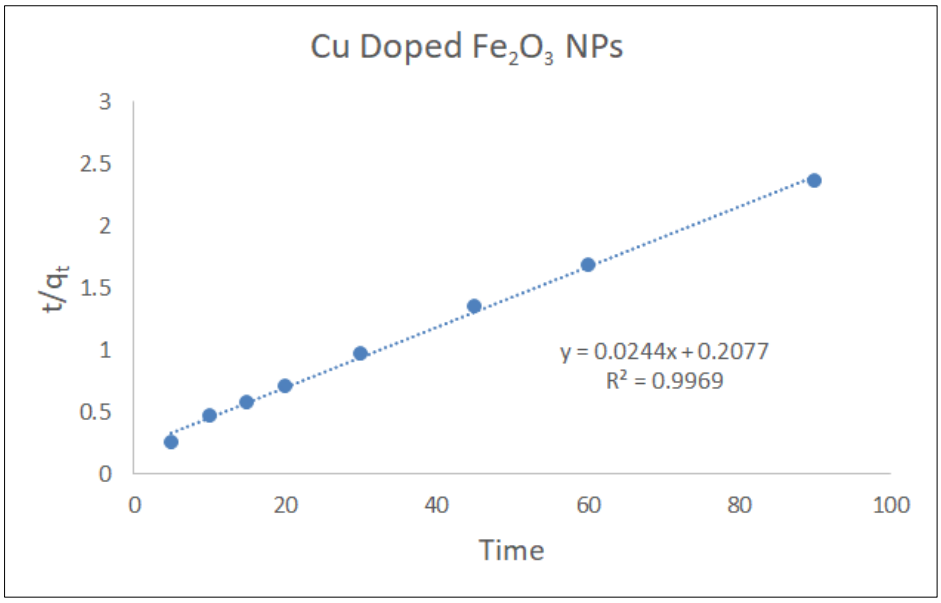

Fig. 13: Pseudo 2nd Order Model

3.9.3 The Kinetic Model of Intraparticle Diffusion

Acid blue-93 molecules must go through many steps to adsorb from liquid media onto adsorbents. The adsorption of Cu-doped Fe_2O_3 nanoparticles on the surface of acid blue-93 may be divided into three basic parts using intra-particle diffusion mechanisms. To transfer adsorbate molecules from the bulk stage to the acid blue-93 exterior, the first method uses diffusion of molecules, sometimes mentioned to as film or diffusion from outside (Wang and Guo, 2022). Adsorbent molecules migrate from the acid blue-93 surface to the interior during the second step of internal diffusion. Adsorbent molecules from the inner area are then absorbed onto the internal pore surfaces in the following phase. The following is the formula for the intra-particle diffusion model:

$$q_t = K_{pi}\, t^{1/2} + C_i \quad (8)$$

In this case, Ci symbolizes the thickness and Kpi the intraparticle diffusion rate constant. The values can be derived by graphing the t-intercept and the slope of the qt versus $t^{1/2}$ plot, respectively.

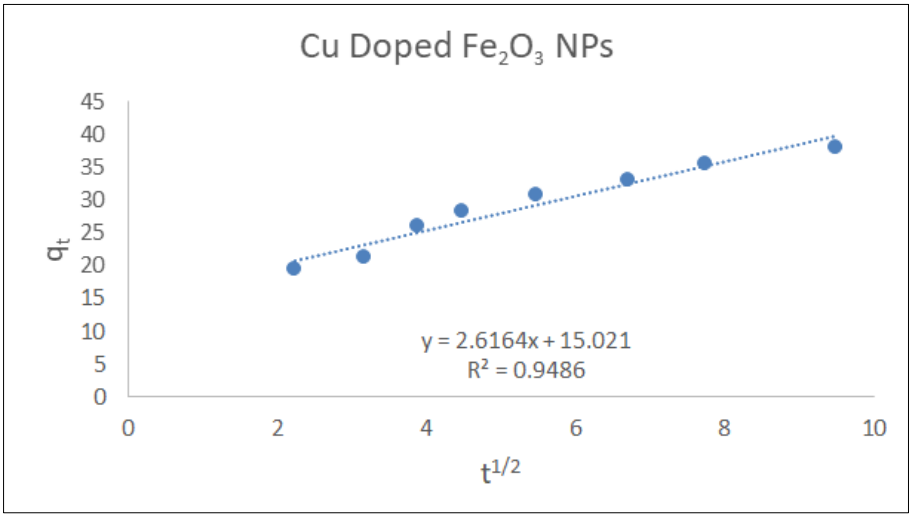

Fig. 14: Intra Particle Diffusion Model

Table 4: Comparison of Kinetic Models

	Pseudo1st order			Pseudo2nd order			IPD		
q_e (exp) (mg/g)	q_e (cal) (mg/g)	K_1 (min^{-1})	R^2	q_e (cal) (mg/g)	K_2 (g $mg^{/}$min)	R^2	KPi	C_i	R^2
38.027	21.07	0.0345	0.9933	40.98	0.003329	0.999	2.61	15.021	0.9486

R^2=1 indicates that a kinetic model of pseudo-2nd order might be used to describe the kinetic data in Table 4. The pseudo-second-order kinetic model outperformed the others, according to the kinetic data analysis. Of the adsorbents examined for the removal of the AB-93 dye, the Intraparticle diffusion model had the lowest correlation value (R^2). Conversely, the pseudo-first-order model showed superior results compared to the Intraparticle diffusion model, but the pseudo-second-order kinetic model surpassed both of them.

3.10 Adsorption Isotherms

The adsorption isotherm, together with the total concentration in the test solution at equilibrium and a steady temperature, explains the connection between a certain unit of adsorbent and the amount of adsorbate adsorbed. Several adsorption isotherms, which are described below, can be used to assess the equilibrium adsorption outcomes of experiments.

3.10.1 Langmuir Adsorption Isotherm

The Langmuir isotherm suggests that a monolayer forms when adsorbates in the liquid phase attach to the surface of Acid Blue 93, which has a limited number of active sites available for attachment. Once the monolayer is formed, no additional adsorbates can occupy the already occupied sites. (Langmuir, 1918) is the linear equation that represents the Langmuir isotherm.

$$C_e/q_e = 1/(mb) + C_e \quad (9)$$

R_L, a significant component of this isotherm, can be computed using the formula below:

$$R_L = 1/(1 + bC_o) \quad (10)$$

Here, the initial concentration of the dye represented by symbol C_o. In this case, b stands for the Langmuir constant, while R_L is the equilibrium parameter. The value of R_L helps determine the adsorption's nature, with R_L = 0 indicating no adsorption, R_L = 1 indicating unfavorable adsorption, R_L = 1 indicating linear adsorption, or R_L < 1 indicating favorable adsorption. The values of qm and b can be derived from the slope and intercept of the graph plotting C_e/q_e against C_e. (Mabuza *et al.*, 2022).

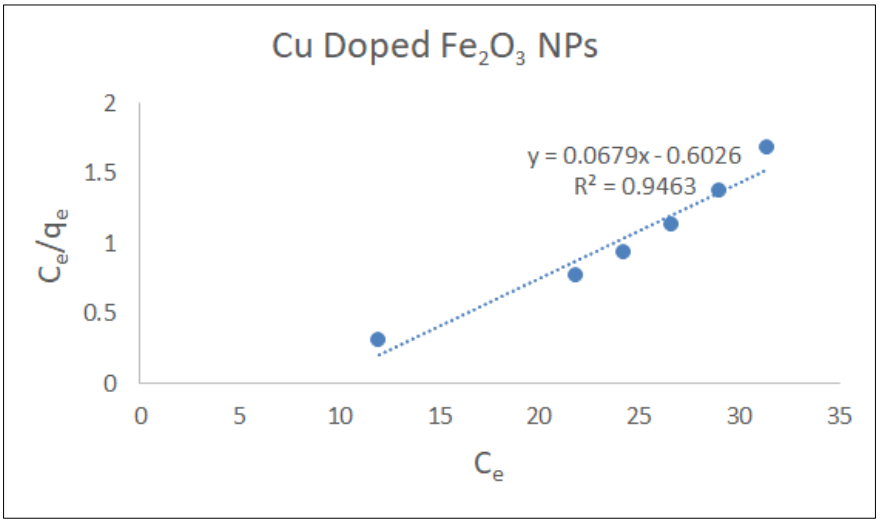

Fig. 15: Langmuir adsorption Isotherm

3.10.2 Freundlich Adsorption Isotherm

According to the Freundlich adsorption isotherm, multiple layers form during the adsorption process. The following is the Freundlich adsorption isotherm's linear equation:

$$\log q_e = \log K_F + (1/n) \log C_e \quad (11)$$

The equilibrium dye concentration (C_e) and adsorption capacity (q_e) are reported in (mgg^{-1}) and (mgL^{-1}), respectively, whereas (K_F) the Freundlich isotherm constant is expressed in (mg/g) $(L/mg)^{1/n}$. The term n represents the intensity of adsorption. The Freundlich isotherm incorporates empirical constants, indicating that these constants' values can vary based on several factors. A value of n=1 indicates a linear adsorption process, a chemical adsorption process is indicated by a value of n < 1, and a value of n greater than one indicates the possibility for adsorption technology (Debnath and Das, 2023). Plotting log q_e against log C_e in the proper order and then figuring out the intercept and slope of the resulting linear graph will yield K_F and n.

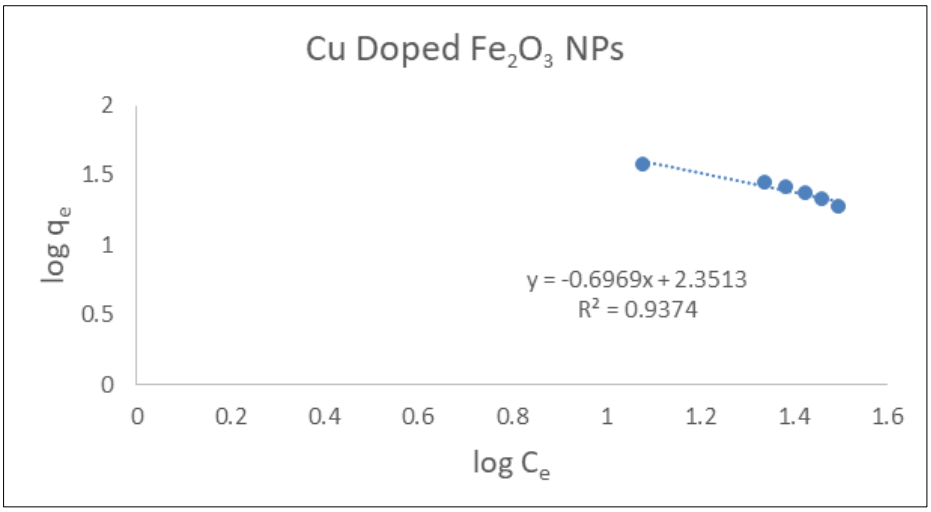

Fig. 16: Freundlich Adsorption Isotherm

3.10.3 Temkin Adsorption Isotherm

Two fundamental presumptions form the basis of the Temkin adsorption isotherm. Based on the 1st presumption, the adsorbent's surface area and the heat required for adsorption are linearly related. Following is the linear equation for Temkin sorption isotherm:

$$q_e = BlnA + BlnC_e \quad (12)$$

R, T, and b are all associated with the Temkin adsorption isotherm represented in the equation B=RT/b, where T denotes the absolute temperature (K) and R denotes the universal gas constant (8.314 J mol^{-1} K^{-1}). Meanwhile, B signifies the constant associated with adsorption heat (J/mol), and A represents the Temkin equilibrium binding constant (L/mg). Plotting the q_e vs. ln C_e graph precisely will get the values for A and B.

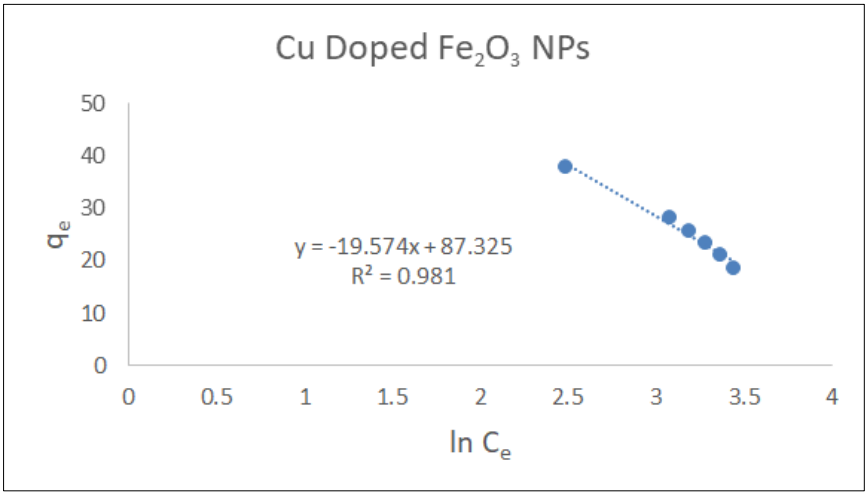

Fig. 17: Tempkin Adsorption Isotherm

3.10.4 Harkins–Jura Adsorption Isotherm

According to the adsorption isotherm proposed by Harkins and Jura, the adsorption process is characterized by the formation of many sorbate layers on the surface of the adsorbent due to the arrangement of the unequal pores. The following is the expression for this model's linear representation:

$$1/q_e^2 = (B/A) - (1/A)logC_e \quad (13)$$

In this equation, B denotes the isotherm's constant and A denotes the Harkins-Jura isotherm's parameter.

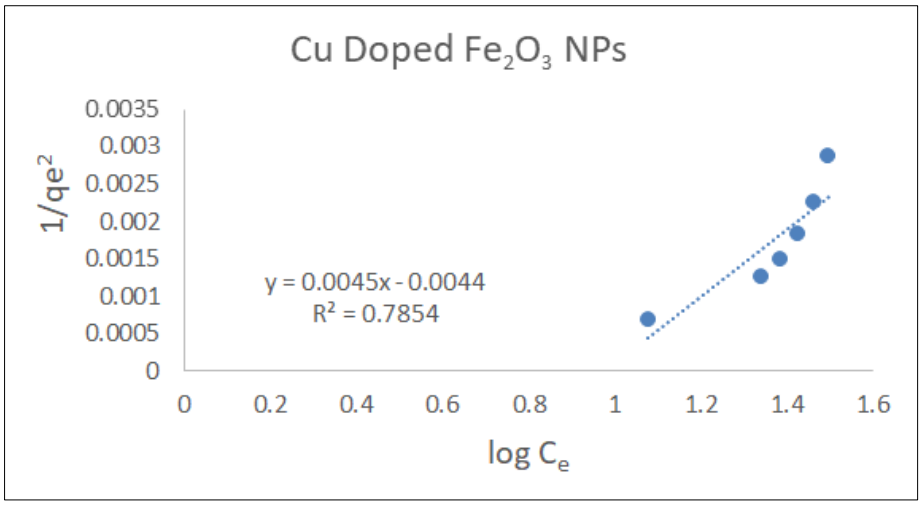

Fig. 18: Harkins-Jura Adsorption Isotherm

3.10.5 Doubinin-Radushkevich (D-R) model

The (D-R) adsorption isotherm can be used to evaluate absorbance characteristics and apparent free E (Doubinin and Radushkevich, 1947). The linear expression of (D-R) sorption isotherm is shown below:

$\ln q_e = \ln q_m - \beta\varepsilon^2$ (14)

In this equation, qm represents the theoretical saturation capacity, a potential that is linked to concentration and is calculated using the given equation, along with the constant representing adsorption energy.

$\varepsilon = RT \ln(1 + 1/C_e)$ (15)

In this context, the absolute temperature and the universal gas constant are denoted by R (8.314 J mol^{-1} K^{-1}) and T (in Kelvin). To determine q_m using m and C values, a plot of ln q_e against ε^2 should be created. The following formula can be employed to determine the mean free energy of adsorption, E:

$E = 1 / (2\beta)^{1/2}$ (16)

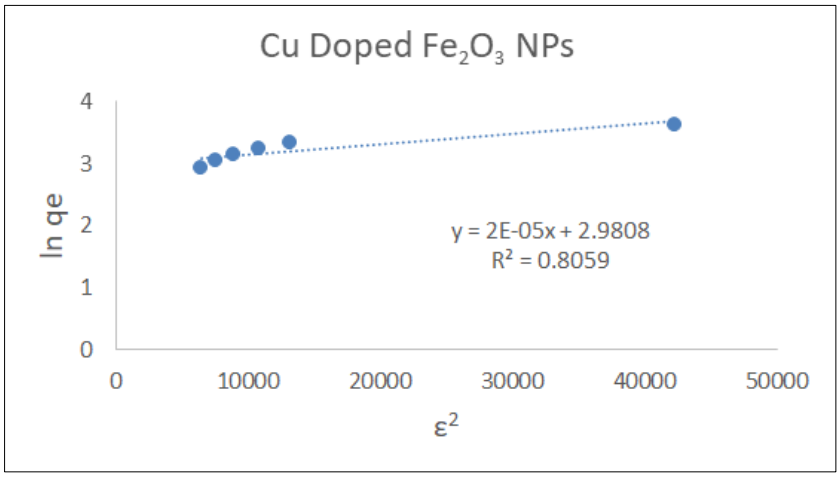

Fig. 19: D-R Adsorption Isotherm

Table 5: Comparison of Equilibrium Models

	Langmuir model				**Freundlich model**		
q_e (exp) (mg/g)	**q_e (cal) (mg/g)**	**KL (L/mg)**	**R^2**	**q_e (cal) (mg/g)**	**K_F (mg/g)**	**1/n**	**R^2**
38.02	14.72	-1.798	0.94	39.80	224.513	0.69	0.93
	Tempkin Model				**Harkins Jura Model**		
q_e (cal) (mg/g)	**A**	**B**	**R^2**	**q_e (cal) (mg/g)**	**A**	**B**	**R^2**
38.72	0.011	-19.57	0.98	47.04	222..2	0.97	0.78

	D-R Model		
q_e cal (mg/g)	**q_m cal (mg/g)**	**E(kJ/mol)**	**R^2**
38.72	8.46	115.11	0.80

The Freundlich model is best for the Cu doped Fe_2O_3 due to similarity between q_e(exp) and q_e(cal). The lower R^2 values made the Harkins-Jura inapplicable.

3.11 Thermodynamic Studies

Analyzing thermodynamics is crucial for comprehending the characteristics of absorbance phenomena. The parameters' values, including (G^o), (H^o), and (S^o), were determined using absorbance measurements while employing Cu-doped Fe_2O_3 nanoparticles as adsorbents to eliminate acid blue-93 dye. The equation below was utilized to derive the Go values for the acidic dye across various temperatures.

$\Delta G^o = \Delta H^o - T\Delta S^o$ (17)

$\Delta G^o = -RT\ln K_d$ (18)

In this context, R refers to the gas constant (8.314 J/mol K^{-1}), T represents the absolute temperature and K_d signifies the thermodynamic equilibrium constant (q_e/C_e). The values of S^o and H^o for Acid Blue-93 were obtained by graphing the relationship between 1/T and ln K_d using the Van 't Hoff equation, subsequently calculating the slope and intercept.

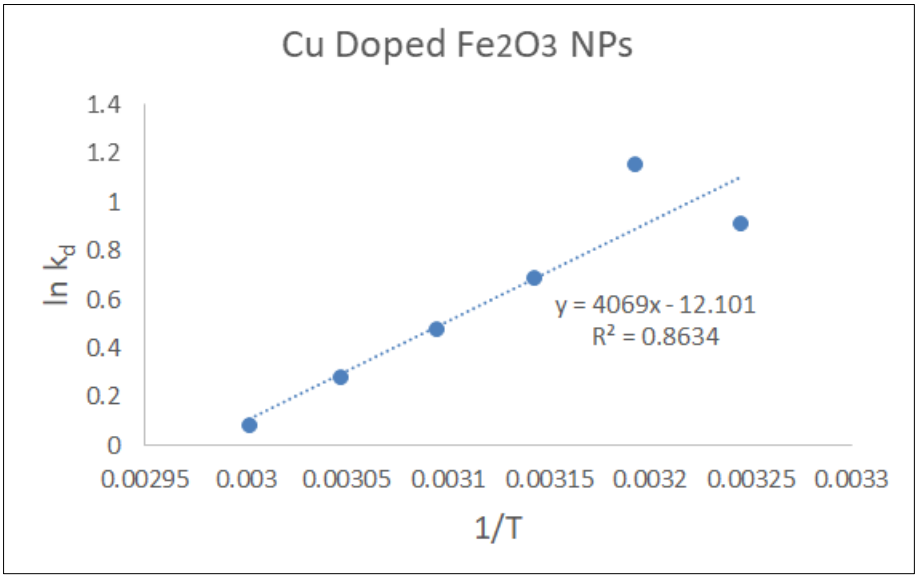

Fig. 20: Thermodynamic studies of Cu/Fe_2O_3 NPs

Table 6: Acid Blue 93 dye removal thermodynamic parameters

Cu/Fe_2O_3 NPs	308	313	318	323	328	333
ΔG° (kJ mol^{-1})	2.28	2.96	1.78	1.25	0.74	0.233
ΔH° (KJ mol^{-1})	28.74					
ΔS°(Jmol^{-1} K^{-1})	-85.94					

The thermodynamic parameter values are presented in Table 6; all adsorption procedures for the elimination of anionic dye are exothermic was illustrated by the negative H° values seen for acidic dye across all types of adsorbents. In each adsorption process aimed at eliminating anionic dyes using Cu-doped Fe_2O_3 as an adsorbent, the solid-liquid interface appeared to be less disordered, as indicated by the low S° values. The propensity for G° values to be negative shows that the adsorption of anionic dye onto the adsorbent occurs concurrently.

3.12 Electrolyte Effects on Acid Blue-93 Dye Adsorption

Salts are widely used in various dyeing techniques within the textile industry. Therefore, the concentration of electrolytes in textile wastewater is important because it affects both the electrostatic and non-electrostatic relation between adsorbent surface and dye molecules, which ultimately affects the adsorbent's effectiveness in dye removal. The effects of several electrolyte concentrations (0.1-0.5M), such as NaCl, $CaSO_4$, and $CuSO_4$, was taken into account in the study on the removal of the dye Acid Blue-93 using the most efficient adsorbent (Cu/Fe_2O_3 NPs). The results indicated that increasing electrolyte concentrations reduced the adsorption capacity of the adsorbent (Cu/Fe_2O_3 NPs) for the corresponding acid dye. This reduction may be attributed to the electrolyte ions obstructing the electrostatic attraction between the dye molecules and the oppositely charged adsorbent molecules.

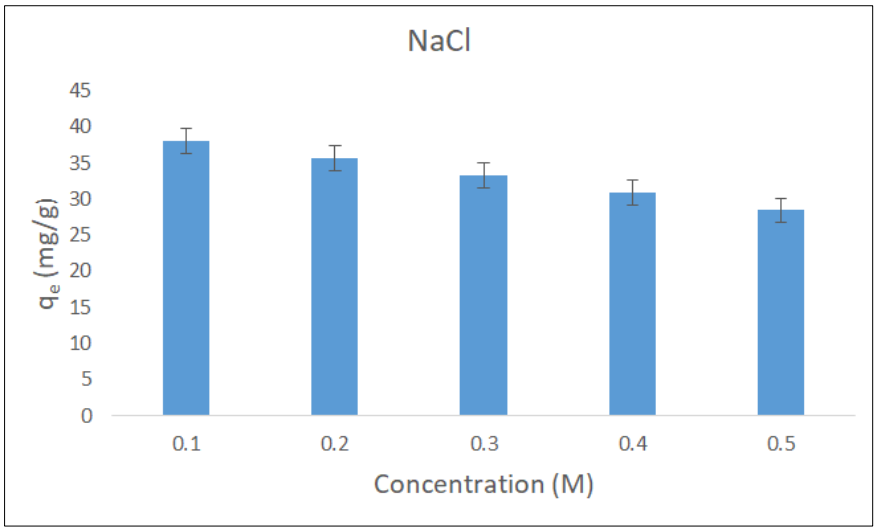

Fig. 21: Effect of NaCl

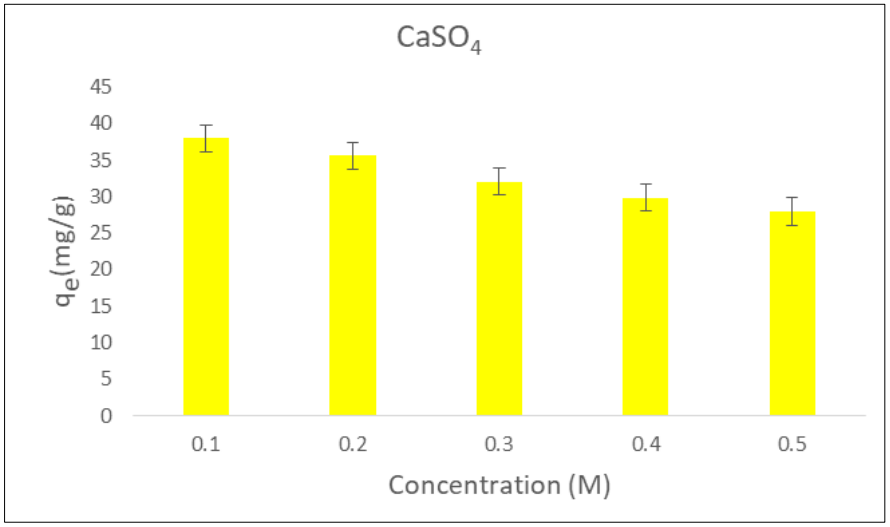

Fig. 22: Effect of CaSO4

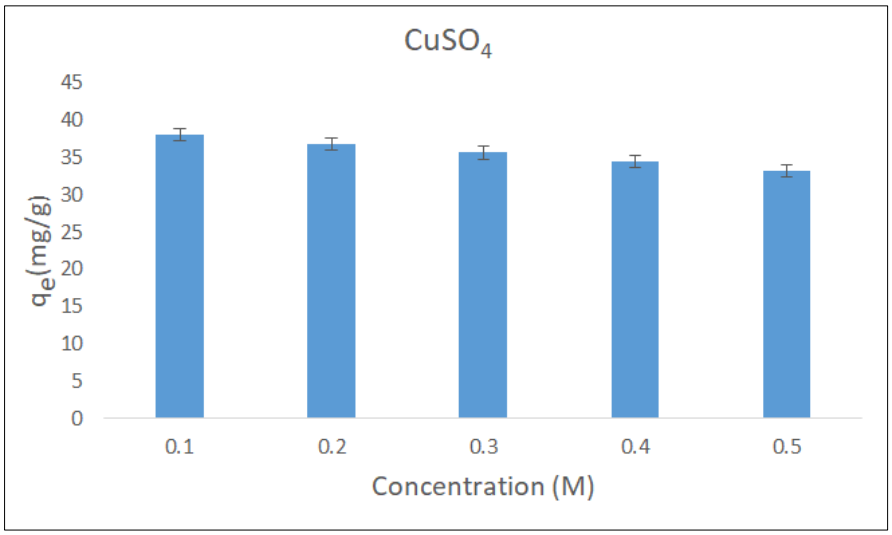

Fig. 23: Effect of CuSO4

3.13 Heavy Metal Ion Effects on AB-93 Dye Adsorption

The adsorption capability was also demonstrated to be significantly impacted by the presence of heavy metal ions in textile effluent. The adsorption capacity of Acid Blue-93 dye rose when heavy metal ions Pb and Cd were introduced to the adsorption medium; on the other hand, the adsorption potential of Acid Blue-93 dye dropped when heavy metal ions were added to the adsorption medium. This aided in assessing the effectiveness of the top adsorbents in removing AB-93.

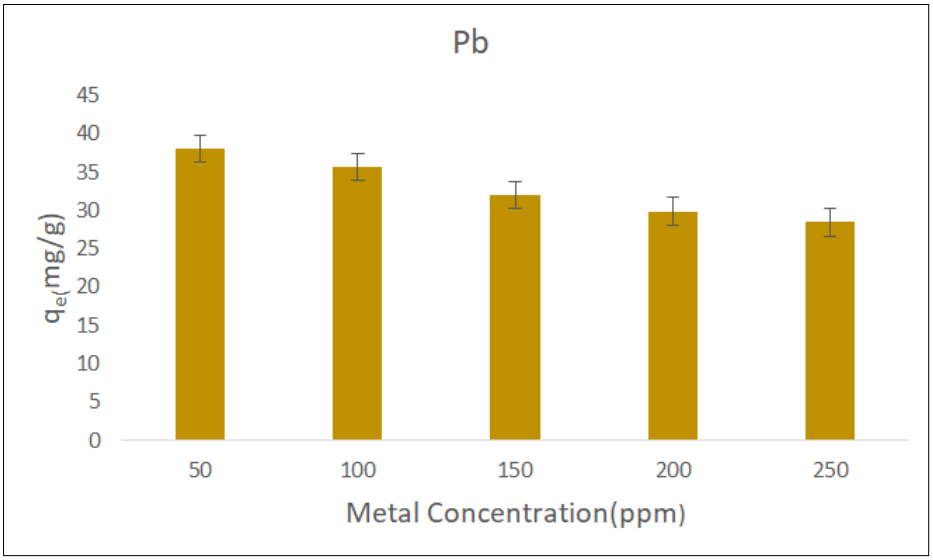

Fig. 24: Effect of Pb

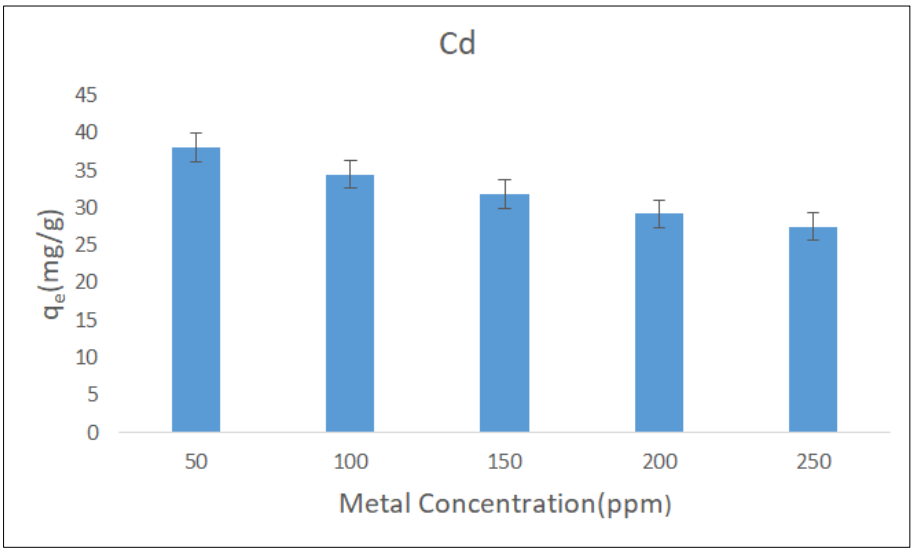

Fig. 25: Effect of Cd

The presence of heavy metal ions may boost Acid Blue-93's adsorption because the dye molecules aggregate and become less soluble, increasing the dye's bioavailability. However, the adsorbent's capacity to further adsorb is reduced when heavy metal ions fill its active binding sites.

3.14 Effects of Detergents and Surfactants on AB-93 Dye Adsorption

The use of surfactants and detergents in the fabric industry may impair the adsorption efficiency of adsorbents. The ability of various detergents (Excel and Arial) and surfactants (SDS, Triton X-100 to remove dye from one percent water-based solutions of Acid Blue 93 was investigated. The results demonstrated that adding several surfactants and detergents considerably reduced Cu/Fe_2O_3 NPs' capacity to adsorb AB-93 dye from the aqueous solution.

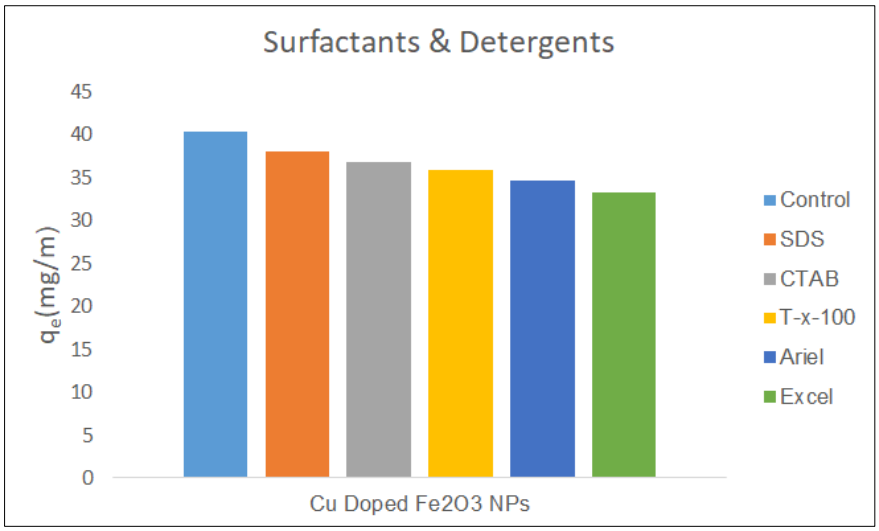

Fig. 26: Effect of Detergents and Surfactants

Based on the results of the experiment, adding the anionic surfactant SDS considerably reduced the adsorbent's ability to adsorb the AB-93 dye it came into contact with. The electrical repulsion of the dye anions by the SDS molecules is a feasible justification for this. It was identified that adding SDS to the AB-93 dye solution significantly decreased the ability of adsorbent to hold onto the dye. Since SDS was also a component of the patch, this was the condition we were interacting with.

3.15 Desorption Study

Investigation into desorption helps understand the adsorption process and increases process effectiveness. An important factor to take into account is choosing a suitable eluent. In this experiment, iron oxide nanoparticles doped with copper proved to be the most efficient adsorbent. A chosen acidic dye was desorbed from this material utilizing two different eluents (NaOH and NH_4OH) at a concentration of 0.5 N. The outcomes showed how the most efficient adsorbents may be used with two eluents to generate varying percentages of acidic dye desorption. Using NaOH and NH_4OH as catalysts caused the largest percentage of desorption, perhaps leading to the dissociation of the adsorbed AB-93 molecules, because of the highest electrical repulsion between the molecules and the adsorbent.

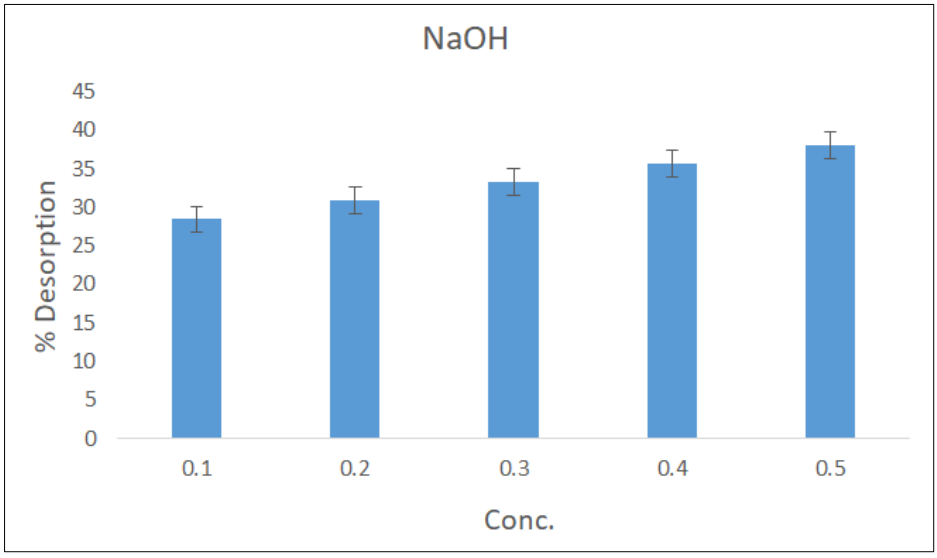

Fig. 27: Effect of NaOH

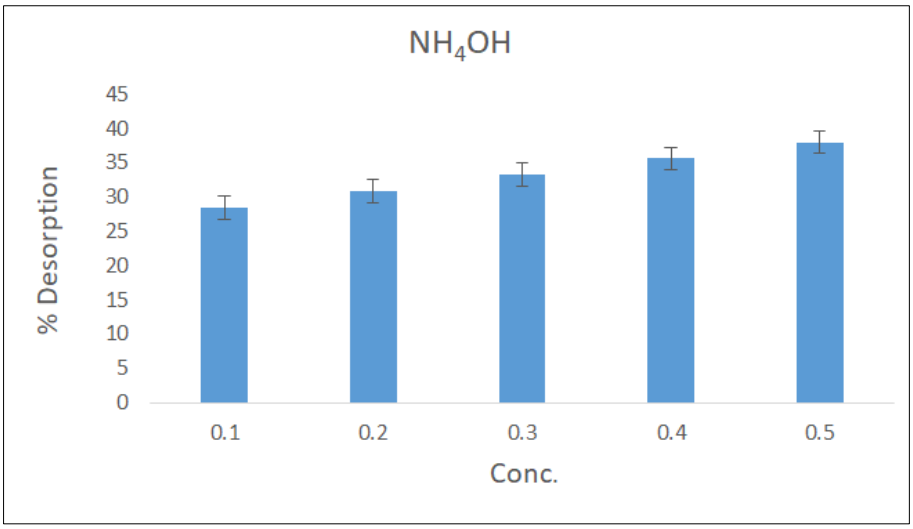

Fig. 28: Effect of NH4O

CONCLUSION

Water is essential for animal life and growth since it covers around 71% of the planet's surface area. Contamination of our water supply is one of the greatest critical problems in the current creation. Due to the numerous chemicals it carried, coloured wastewater was very dangerous for people, animals, and marine life. Recent studies reveal that AB 93 dye may be greatly diluted or even completely removed from a solution using Cu/Fe_2O_3 nanoparticles. To achieve the desired outcomes, a number of parameters, including adsorbent dosage, contact time, pH, and beginning dye concentration, must be adjusted. The pseudo-2nd order model and Freundlich adsorption isotherm provided a good explanation for the AB-93 dye data. To examine the characteristics and viability of the adsorption process, several thermodynamic parameters were evaluated. The maximum desorption of acidic dyes was achieved using 0.5 N NaOH and 0.5 N NH_4OH for AB-93. FT-IR and XRD techniques were used for characterization. For treating wastewater contaminated with acidic dye, the metal doped nanoparticles mentioned are recognized as the materials that are most economical, sustainable, ecologically benign, and environmental friendly.

Future Perspectives

Using Cu-doped Fe_2O_3 nanoparticles (NPs) as an adsorbent to remove dye from wastewater requires controlling the size, shape, and surface characteristics of the particles through optimal manufacturing methods. Sustainability requires improving regeneration and reusability with an emphasis on stability and desorption efficiency. For practical uses, selectivity in intricate wastewater matrices including several pollutants must be investigated. Cu-doped Fe_2O_3 NPs may be more effective when combined with other treatment technologies such as membrane filtration and photo catalysis. Safety must be guaranteed by environmental and toxicological evaluations that take leaching potential and biodegradability into account. For industrial deployment, pilot-scale studies are required to assess feasibility and cost-effectiveness. Adsorption capacity may be further increased by functionalization or incorporation into hybrid materials, such as polymer composites and graphene-based structures. By addressing these factors, their growth into effective, environmentally friendly wastewater treatment systems will be aided.

Highlights

1. Cu-doped Fe_2O_3 nanoparticles were synthesized using a straightforward co-precipitation technique.
2. Cu ions were effectively doped in Fe_2O_3, as shown by FTIR and XRD measurements.
3. Pseudo 2nd order kinetic and Freundlich model fits the experimental data rather well.
4. Cu-doped Fe_2O_3 nanoparticles' ability as adsorbent was used to degrade AB-93 dye.

REFERENCES

- Aashima *et al.* (2019) 'Magnetically retrievable Ce-doped Fe3O4 nanoparticles as scaffolds for the removal of azo dyes', *RSC Advances*, 9(40), pp. 23129–23141. Available at: https://doi.org/10.1039/c9ra03252e.
- Abel, S. *et al.* (2021) 'Application of Titanium Dioxide Nanoparticles Synthesized by Sol-Gel Methods in Wastewater Treatment', *Journal of Nanomaterials*, 2021, pp.1-6. Available at: https://doi.org/10.1155/2021/3039761.
- Asfaram, A. *et al.* (2017) 'Screening and optimization of highly effective ultrasound-assisted simultaneous adsorption of cationic dyes onto Mn-doped Fe3O4-nanoparticle-loaded activated carbon', *Ultrasonics Sonochemistry*, 34, pp. 1–12. Available at: https://doi.org/10.1016/j.ultsonch.2016.05.011.
- Chen, W. *et al.* (2019) 'Enhanced removal of lead ions from aqueous solution by iron oxide nanomaterials with cobalt and nickel doping', *Journal of Cleaner Production*, 211, pp. 1250–1258.

Available at: https://doi.org/10.1016/j.jclepro.2018.11.254.

- Deng, D. *et al.* (2020) 'Textiles wastewater treatment technology: A review', *Water Environment Research*, 92(10), pp. 1805–1810. Available at: https://doi.org/10.1002/wer.1437.
- El-Habacha, M. *et al.* (2023) 'An efficient and adsorption of methylene blue dye on a natural clay surface: modeling and equilibrium studies', *Environmental Science and Pollution Research*, pp. 1-15. Available at: https://doi.org/10.1007/s11356-023-27413-3.
- Haider, S. *et al.* (2022) 'Visible light active Cu-doped iron oxide for photocatalytic treatment of methylene blue', *Ceramics International*, 48(6), pp. 7605–7612. Available at: https://doi.org/10.1016/j.ceramint.2021.11.304.
- Harish, V. *et al.* (2022) 'Nanoparticle and Nanostructure Synthesis and Controlled Growth Methods', *Nanomaterials*, 12(18), pp. 1–30. Available at: https://doi.org/10.3390/nano12183226.
- Jain, K. *et al.* (2021) 'Nanotechnology in Wastewater Management: A New Paradigm Towards Wastewater Treatment', *Molecules*, 26(6), p. 1797-1822. Available at: https://doi.org/10.3390/molecules26061797.
- Jang, S.H. *et al.* (2022) 'Synthesis and characterisation of triphenylmethine dyes for colour conversion layer of the virtual and augmented reality display', *Dyes and Pigments*, 204(January), p. 110419-110427. Available at: https://doi.org/10.1016/j.dyepig.2022.110419.
- Kiani, M. *et al.* (2019) 'Adsorption of purpurin dye from industrial wastewater using Mn-doped Fe2O4 nanoparticles loaded on activated carbon', *Desalination and Water Treatment*, 152, pp. 366–373. Available at: https://doi.org/10.5004/dwt.2019.23694.
- Lafi, R., Montasser, I. and Hafiane, A. (2019) 'Adsorption of congo red dye from aqueous solutions by prepared activated carbon with oxygen-containing functional groups and its regeneration', *Adsorption Science & Technology*, 37(1–2), pp. 160–181. Available at: https://doi.org/10.1177/0263617418819227.
- Liang, X. *et al.* (2010) 'The remarkable effect of vanadium doping on the adsorption and catalytic activity of magnetite in the decolorization of methylene blue', *Applied Catalysis B: Environmental*, 97(1–2), pp. 151–159. Available at: https://doi.org/10.1016/j.apcatb.2010.03.035.
- Liu, L. *et al.* (2021) 'Treatment of industrial dye wastewater and pharmaceutical residue wastewater by advanced oxidation processes and its combination with nanocatalysts: A review', *Journal of Water Process Engineering*, 42(22), p. 102122-102140. Available at: https://doi.org/10.1016/j.jwpe.2021.102122.
- Mabuza, M., Premlall, K. and Daramola, M.O. (2022) 'Modelling and thermodynamic properties of pure CO2 and flue gas sorption data on South African coals using Langmuir, Freundlich, Temkin, and extended Langmuir isotherm models', *International Journal of Coal Science and Technology*, 9(1), pp.1-15. Available at: https://doi.org/10.1007/s40789-022-00515-y.
- McCall, C. *et al.* (2020) 'Identification of multiple potential viral diseases in a large urban center using wastewater surveillance', *Water Research*, 184, p. 116160-116172. Available at: https://doi.org/10.1016/j.watres.2020.116160.
- Mok, C.F. *et al.* (2020) 'Adsorption of Dyes Using Poly(vinyl alcohol) (PVA) and PVA-Based Polymer Composite Adsorbents: A Review', *Journal of Polymers and the Environment*, 28(3), pp. 775–793. Available at: https://doi.org/10.1007/s10924-020-01656-4.
- Mozaffari Majd, M. *et al.* (2022) 'Adsorption isotherm models: A comprehensive and systematic review (2010−2020)', *Science of the Total Environment*, 812, pp. 151334-151361. Available at: https://doi.org/10.1016/j.scitotenv.2021.151334.
- Muthukumaran, P. *et al.* (2022) 'Polymeric biomolecules based nanomaterials: Production strategies and pollutant mitigation as an emerging tool for environmental application', *Chemosphere*, 307(P4), pp. 136008-1360024. Available at: https://doi.org/10.1016/j.chemosphere.2022.136008.
- Pirsaheb, M. *et al.* (2019) 'Photocatalyzed degradation of acid orange 7 dye under sunlight and ultraviolet irradiation using Ni-doped ZnO nanoparticles', *Desalination and Water Treatment*, 165, pp. 321–331. Available at: https://doi.org/10.5004/dwt.2019.24462.
- Raza, A. *et al.* (2022) 'Phoenix dactylifera mediated green synthesis of Mn doped ZnO nanoparticles and its adsorption performance for methyl orange dye removal: A comparative study', *Materials Chemistry and Physics*, 286(October 2021), pp. 126173-126185. Available at: https://doi.org/10.1016/j.matchemphys.2022.126173.
- Rehman, A.U. *et al.* (2022) 'Green synthesis of manganese-doped superparamagnetic iron oxide nanoparticles for the effective removal of Pb(ii) from aqueous solutions', *Green Processing and Synthesis*, 11(1), pp. 287–305. Available at: https://doi.org/10.1515/gps-2022-0030.
- Sohail, M.T. *et al.* (2022) 'Investigating the Drinking Water Quality and Associated Health Risks in Metropolis Area of Pakistan', *Frontiers in Materials*, 9(April), pp. 1–8. Available at: https://doi.org/10.3389/fmats.2022.864254.
- Sooch, B.S., Mann, M.K. and Sharma, M. (2021) 'Metal-Doped Barium Sulphate Nanoparticles Decorated with Gelatin as Antibacterial Agents', *Journal of Cluster Science*, 32(5), pp. 1141–1154. Available at: https://doi.org/10.1007/s10876-020-

01878-5.

- Tran, H.N. (2023) 'Applying Linear Forms of Pseudo-Second-Order Kinetic Model for Feasibly Identifying Errors in the Initial Periods of Time-Dependent Adsorption Datasets', *Water (Switzerland)*, 15(6), pp. 1-14. Available at: https://doi.org/10.3390/w15061231.
- Wang, J. and Guo, X. (2022) 'Rethinking of the intraparticle diffusion adsorption kinetics model: Interpretation, solving methods and applications', *Chemosphere*, 309(P2), pp. 136732-136743. Available at: https://doi.org/10.1016/j.chemosphere.2022.136732.
- Yildiz, S. *et al.* (2023) 'Experimental and density functional theoretical analyses on degradation of acid orange 7 via UV irradiation and ultrasound enhanced by fenton process', *Journal of Molecular Structure*, 1277, pp. 134833-134843. Available at: https://doi.org/10.1016/j.molstruc.2022.134833.
- Zhang, H. *et al.* (2022) 'Spatial and temporal dynamics of actinobacteria in drinking water reservoirs: Novel insights into abundance, community structure, and co-existence model', *Science of the Total Environment*, 814, pp. 152804-152818. Available at: https://doi.org/10.1016/j.scitotenv.2021.152804.